Microphase Ordering Mechanisms in Linear ABC Triblock Copolymers. A Dynamic Density Functional Study

Jianfeng Xia, Mingzhu Sun, Feng Qiu,* Hongdong Zhang, and Yuliang Yang

The Key Laboratory of Molecular Engineering of Polymers, Ministry of Education, China, Department of Macromolecular Science, Fudan University, Shanghai 200433, China

Received June 25, 2005; Revised Manuscript Received August 12, 2005

ABSTRACT: The microphase ordering processes for ABC linear triblock copolymers are investigated using dynamic density functional theory (DDFT). The implementation of the DDFT is verified by comparing the 2D equilibrium triblock morphologies it predicted with previous theory and experiments. Quenched from a disordered state, the microphase separation of the ABC triblock copolymers may proceed through either one-step or two-step ordering mechanism, depending on the composition and the interaction energies of the three components. When the volume fraction of one species dominates the other two, the microphase ordering always proceeds through a two-step mechanism with the majority one segregating at first, provided a three-phase morphology formed at the end. When the volume fractions of the three species are comparable, for the symmetric interaction case, the microphase separation occurs through a one-step mechanism, while for the asymmetric interaction case, it occurs through a two-step mechanism with the most incompatible species segregating at first.

I. Introduction

Block copolymers, which are macromolecules comprising blocks that differ in chemical nature, have a fascinating ability to form a rich variety of nanoscale, periodic morphologies, which offers great potential in developing materials with nanoscale structures ranging from nanoreactors to photonic crystals.[1] In the past decades, experiments[2−4] and theories[5−8] have focused on equilibrium block copolymer morphologies. For AB diblock copolymers, it has been recognized that four stable microphases—spheres, cylinders, gyroid, and lamellae—exist under equilibrium conditions.[9] Recently, an O^{70} network phase was also predicted to be stable in diblock copolymer melts by field theoretic calculation.[10] The driving force for the formation of these morphologies comes from minimizing the stretching energy, originating from the A and B domains due to the connectivity of the A and B blocks, and the interfacial energy, arising from the energetically unfavorable contacts between the A and B monomers.

The long-range interactions and large relaxation times involved in block copolymer melts make the mechanism of phase transformation richer and more interesting. Furthermore, the study of the order−disorder transition (ODT) or order−order transition (OOT) in block copolymers is helpful in designing suitable processing routes for obtaining specific well-ordered structures. Therefore, the kinetics of phase separation in diblock copolymers has been extensively studied in experiments and theory. Bates and coworkers first presented the complex phase behavior near the ODT using a series of poly(ethylenepropylene-*b*-ethylethylene) (PEP−PEE)[11] and poly(styrene-*b*-isoprene) (PS−PI) diblock copolymers.[12,13] They identified new morphologies such as the hexagonally perforated layers (HPL) and the bicontinuous cubic phase having an $Ia\bar{3}d$ space group symmetry (gyroid). Recently, a reversible change between hexagonally arranged cylinders and bcc spheres was observed in PS−PI diblock copolymers, which involves a mechanism that the cylinders are transformed into a series of spheres with the cylinder axes corresponding to the [111] direction of the bcc spheres upon heating, while upon cooling these spheres are deformed and interconnected to form cylinders.[14]

Computer simulations on kinetics of diblock copolymer phase separation were mainly carried out by cell dynamic simulations (CDS) based on the time-dependent Ginzburg−Landau (TDGL) equation. The first CDS for block copolymers was of two-dimensional stripe pattern,[15] which has revealed that hydrodynamic effects are crucial for the late stage ordering processes. Qi and Wang have shown that the pathways of the hexagonal cylinder phase to disordered and bcc sphere phase involve the disappearance of the amplitude of the hexagonal waves and the appearance of bcc waves in ODT and OOT of diblock copolymers.[16] Recently, Hamley et al. systematically investigated the effects of the simulation parameters on the final morphology in three dimensions.[17] They found that sphere, cylinder, bicontinuous, and lamellar morphologies can be generated by the appropriate selection of ordering temperature and copolymer composition.

For triblock copolymers, rich and complex morphologies, such as lamellae−sphere and lamellae−cylinder phases and the "knitting pattern" structure, have been observed.[18−20] However, the mechanisms of how these microphases are formed in triblock copolymers have received less attention until now since it is more complicated than that in diblock copolymers, although such complex phase ordering kinetics arise from the standard competition between the long-range interaction due to the covalent connection among different blocks and their short-ranged chemical incompatibility. Quenched from a disordered state, the possible ordering process for a linear ABC triblock copolymer could be through either a one-step or two-step mechanism, as illustrated in Figure 1. If after a sudden quench the

* To whom correspondence should be addressed. E-mail: fengqiu@fudan.edu.cn.

10.1021/ma051355b CCC: $30.25 © 2005 American Chemical Society
Published on Web 10/01/2005

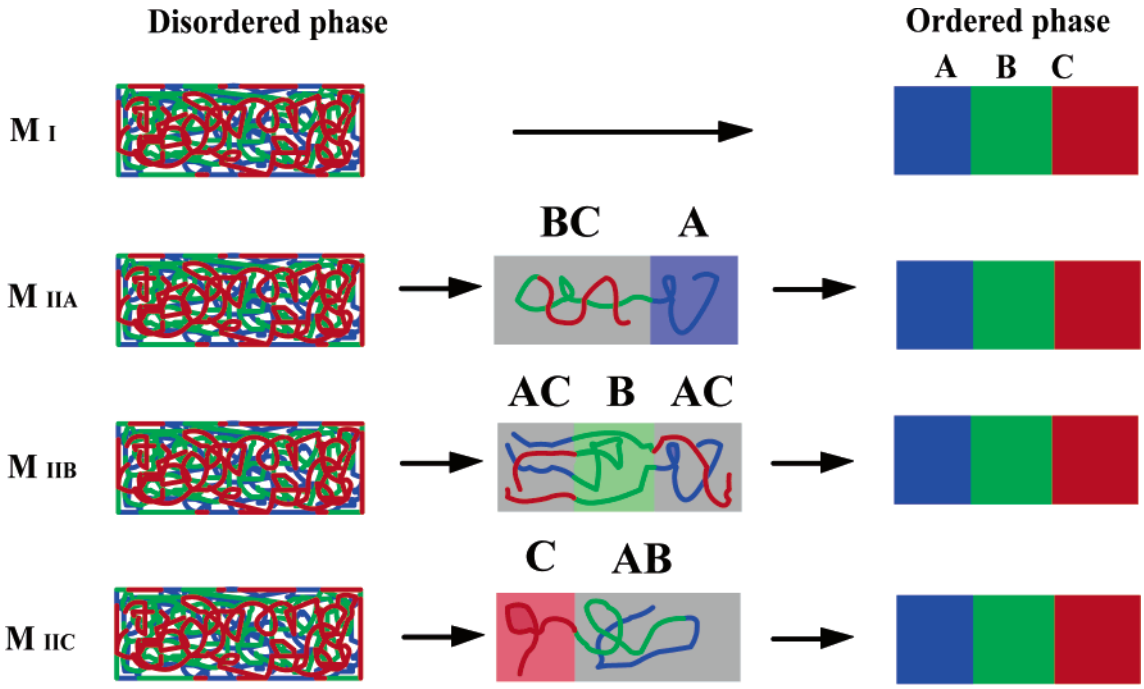

Figure 1. Schematic illustration of possible ordering mechanisms for the disorder-to-order transition in linear ABC triblock copolymer melts. For one-step ordering mechanism, M_I, the three components separate simultaneously. The two-step ordering mechanism is classified into three subtypes: in M_{IIA} and M_{IIC} one end of the triblock (either A or C) separates from the other two blocks first, followed by segregation of the rest two blocks; in M_{IIB} the middle block B separates from the two end blocks first, and then segregation of the two end blocks occurs. Three different colors, blue, green, and red, are assigned to A, B, and C blocks, respectively.

three species separate from each other simultaneously, it is called one-step mechanism, denoted by M_I, while if at first one species segregates from the other two, and then the remaining two mixed species separate from each other, it is a two-step mechanism, M_{II}, which may be further classified into three subcases: M_{IIA}, M_{IIB}, and M_{IIC} (see Figure 1), depending on the compositions and the interaction energies among the three species. The two-step mechanism is of special interests because the self-assembly of each block can be controlled independently, which facilitates assigning different functionalities to different blocks.

Recently, a similar two-step mechanism has been demonstrated by Yamauchi et al. in the microphase separation of a poly(isoprene-*b*-styrene-*b*-vinyl methyl ether) triblock copolymer[21,22] and subsequently analyzed by Maniadis et al. using self-consistent-field theory (SCFT) for triblock copolymers.[23] Both the experiment and theory showed that the two-step mechanism was successfully achieved by changing the interaction energies among the three species through either varying the temperature or adding a selective solvent. Inspired by these works, it is natural to ask whether there are simpler ways to achieve two-step microphase separation and how they are related to the molecular parameters such as the composition of the triblocks and the interaction energies among the different species. A promising theoretical tool to investigate these problems is the dynamic density functional theory (DDFT).

The DDFT for polymers was originally proposed by Fraaije[24,25] and was already used to simulate the kinetics of diblock copolymer melts. It is capable of describing the extremely slow defect annihilation relaxation and the density pattern of the diblocks evolving to metastable states, in which isolated defects separate well-ordered microdomains in the nonlinear regime. The main idea of DDFT is as follows: the kinetics of the system is assumed to obey the TDGL equation, and the chemical potential of the system can be obtained by a trick using hypothetical external fields, which leads to a set of self-consistent nonlinear equations that can be solved by various iteration schemes. Using the Newton−Broyden method, Reister et al. simulated the spinodal decomposition of a binary polymer mixture and found that the results obtained by DDFT can be quantitatively compared with that by Monte Carlo simulation.[26] Yeung and Shi studied the formation of interfaces in incompatible polymer blends using a combination of gradient-descent and secant methods.[27] Their results showed that the interfacial width grows as $t^{1/4}$ at early times and saturates to the equilibrium thickness at long times. Morita et al. investigated the morphology and dynamics of mixture of long and short block copolymers.[28] They clarified that complex domain structures and the mechanism of the phase separation dynamics arise from the competition between the micro- and macrophase separations.

In this paper, we explore possible ordering mechanisms for linear ABC triblock copolymers quenched from a disordered state by using DDFT. The organization of the paper is as follows: In section II, the model equations and algorithm are briefly described. In section III, to confirm the validity of the algorithm, the equilibrium morphology of the linear ABC triblock copolymer in 2D is presented and compared to previous experiments and theories. We then choose the triblocks with different but typical interaction parameters to investigate possible ordering mechanisms involved in the microphase separation. By systematically varying the composition of the system, the ordering mechanism diagrams are constructed. Finally, in section IV, the main conclusions of the present study are given.

II. DDFT Method

We consider a system of n linear ABC triblock copolymers each with chain length N. The volume of the system is V, and the compositions of the triblock copolymer are defined by f_I (I = A, B, C). We choose the DDFT rather than the CDS because the free energy functional obtained for ABC triblock copolymers through the random phase approximation (RPA) is only qualitative.[29] Furthermore, the DDFT takes into account the architectural effect of the polymer chains through the path integral method, in which the polymer chains are modeled as Gaussian chains. The phase separation kinetics of the system is assumed to obey the TDGL equation for the conserved order parameter (model B),[30] without considering the effect of hydrodynamics

$$\frac{\partial \phi_I(\mathbf{r},t)}{\partial t} = L_I \nabla^2 \frac{\delta F[\phi_I(\mathbf{r})]}{\delta \phi_I(\mathbf{r})} + \eta_I(\mathbf{r},t) \tag{1}$$

where $\phi_I(\mathbf{r},t)$ (I = A, B, C) represents the monomer density fields of species I at position $\mathbf{r}$ and time t; L_I is the segment mobility coefficient of species I, which is assumed to be a constant. Here we neglect the dependence of the mobility on the density $\phi_I(\mathbf{r})$, and the entanglement effects are not taken into account. η_I is the Gaussian thermal noise with the zero mean and satisfies the fluctuation−dissipation relation

$$\langle \eta_I(\mathbf{r},t) \rangle = 0 \tag{2}$$

$$\langle \eta_I(\mathbf{r},t)\, \eta_I(\mathbf{r}',t') \rangle = -2L_I k_B T \nabla^2 \delta(\mathbf{r}-\mathbf{r}')\, \delta(t-t') \tag{3}$$

$F[\phi_I(\mathbf{r})]$ is the free energy functional of the system (in the unit of nNk_BT), and then $\delta F[\phi_I(\mathbf{r})]/\delta\phi_I(\mathbf{r})$ represents the chemical potential $\mu_I(\mathbf{r})$ of species I at position $\mathbf{r}$, which can be calculated by the following trick:[31] Since the system described by eq 1 is not in equilibrium, if a hypothetical external field $U_I(\mathbf{r})$ acting on the I species was introduced to exactly cancel the current chemical potential $\mu_I(\mathbf{r})$; i.e., $U_I = -\mu_I$, which makes the current density profile $\phi_I(\mathbf{r},t)$ to be in an equilibrium state. By this way, the question of finding the chemical potential $\mu_I(\mathbf{r})$ changes to finding the hypothetical external field $U_I(\mathbf{r})$, which can be solved in the frame of the self-consistent-field theory (SCFT).

In SCFT, the fundamental quantity to be calculate is the polymer segment probability distribution function, $q(\mathbf{r},s)$, representing the probability of finding segment s at position $\mathbf{r}$. It satisfies a modified diffusion equation[32,33]

$$\frac{\partial q(\mathbf{r},s)}{\partial s} = \frac{a^2}{6}\nabla^2 q(\mathbf{r},s) - [\gamma_A(s)\,\omega_A(\mathbf{r}) + \gamma_B(s)\,\omega_B(\mathbf{r}) + \gamma_C(s)\,\omega_C(\mathbf{r})] q(\mathbf{r},s) \tag{4}$$

where a is the statistical segment length of the polymer and $\omega_I(\mathbf{r})$ is the self-consistent field exerted to the species I, and $\gamma_I(s)$ is 1 if s belongs to block I and 0 otherwise. The initial condition is $q(\mathbf{r},0) = 1$. Because the two ends of the triblock chain are distinct, a second end segment distribution function $q^+(\mathbf{r},s)$ is needed, which satisfies eq 4 only with the right-hand side multiplied by −1, and the initial condition is $q^+(\mathbf{r},N) = 1$. Thus, the single chain partition function Q subject to the mean-field $\omega_I(\mathbf{r})$ can be written as $Q = \int \mathrm{d}\mathbf{r}\, q(\mathbf{r},s)\, q^+(\mathbf{r},s)$ in terms of $q(\mathbf{r},s)$ and $q^+(\mathbf{r},s)$.

The monomer density fields of species I at position $\boldsymbol{r}$ are calculated as

$$\phi_A(\mathbf{r}) = \frac{V}{NQ}\int_0^{f_A N} \mathrm{d}s\; q(\mathbf{r},s)\, q^+(\mathbf{r},s) \tag{5}$$

$$\phi_B(\mathbf{r}) = \frac{V}{NQ}\int_{f_A N}^{(f_A+f_B)N} \mathrm{d}s\; q(\mathbf{r},s)\, q^+(\mathbf{r},s) \tag{6}$$

$$\phi_C(\mathbf{r}) = \frac{V}{NQ}\int_{(f_A+f_B)N}^{N} \mathrm{d}s\; q(\mathbf{r},s)\, q^+(\mathbf{r},s) \tag{7}$$

The hypothetical external field $U_I(\mathbf{r})$ is given by the difference of the mean field created by other polymer segments and the self-consistent-field $\omega_I(\mathbf{r})$ that forces the segment density to a given density profile $\phi_I(\mathbf{r})$

$$U_A(\mathbf{r}) = \omega_A(\mathbf{r}) - \chi_{AB}\phi_B(\mathbf{r}) - \chi_{AC}\phi_C(\mathbf{r}) \tag{8}$$

$$U_B(\mathbf{r}) = \omega_B(\mathbf{r}) - \chi_{AB}\phi_A(\mathbf{r}) - \chi_{BC}\phi_C(\mathbf{r}) \tag{9}$$

$$U_C(\mathbf{r}) = \omega_C(\mathbf{r}) - \chi_{AC}\phi_A(\mathbf{r}) - \chi_{BC}\phi_B(\mathbf{r}) \tag{10}$$

where χ_{IJ} is the dimensionless Flory−Huggins interaction in the unit of k_BT. Equations 4−10 form a closed set of self-consistent equations. The self-consistent-field $\omega_I(\mathbf{r})$ is determined by adjusting it iteratively with the steepest descent method so that the density profiles calculated by eqs 5−7 coincide with that using eq 1. Physically, this self-consistent calculation means that the chain conformations are assumed to be in local equilibrium with the given density profiles. Once the set of self-consistent equations, eqs 4−10, are solved, the chemical potential for the I segment is given by $\mu_I = -U_I$. When it is substituted into eq 1, the density profile is updated.

It should be noted that when solving eq 1, it has to be supplemented by the total incompressibility condition

$$\sum_I \phi_I(\mathbf{r},t) = 1 \tag{11}$$

which implies that the total currents $\sum_I J_I = 0$.[28,34] A common means to enforce the incompressibility of the system is to introduce a potential field $\xi(\mathbf{r})$, which is also known as the Lagrange multiplier. Therefore, the current chemical potential is given by

$$\mu_I(\mathbf{r}) = -U_I(\mathbf{r}) + \xi(\mathbf{r}) \tag{12}$$

where $\xi(\mathbf{r})$ is chosen to be

$$\xi(\mathbf{r}) = \lambda[1 - \phi_A(\mathbf{r}) - \phi_B(\mathbf{r}) - \phi_C(\mathbf{r})] \tag{13}$$

where λ is large enough to ensure the incompressibility of the system and the resulting density profiles and free energy should be independent of its particular value.[35]

III. Results and Discussion

For the sake of numerical tractability, most of calculations are carried out in a two-dimensional 28 × 28 cell with periodic boundary conditions. We have verified that this cell size is sufficient for obtaining accurate enough morphologies and correct phase separation dynamics with the parameters used in the simulation. Larger cell size causes significant increase of computation time and defects which are difficult to be an-

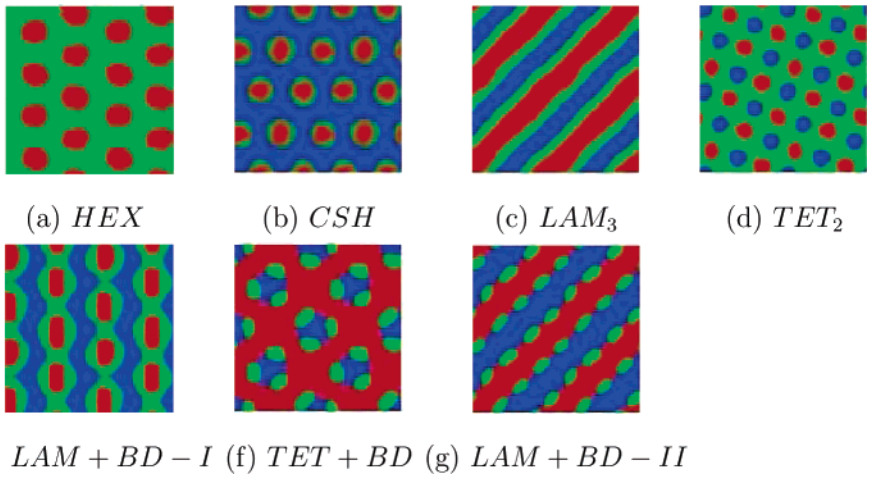

Figure 2. Two-dimensional equilibrium microphases of linear ABC triblock copolymers on a 28 × 28 lattice with periodic boundary condition and chain length $N = 100$. For a clear presentation of the final pattern, the linear dimensions of the cell are replicated two times in each direction. (a) Hexagonal lattice phase (HEX); (b) core−shell hexagonal lattice phase (CSH); (c) "three-color" lamellar phase (LAM_3); (d) two-interpenetrating-tetragonal lattice phase (TET_2); (e) lamellar phase with beads inside (LAM + BD-I); (f) tetragonal phase with beads at interface (TET + BD); (g) lamellar phase with beads at interface (LAM + BD-II).

nihilated. The chain length is fixed to be $N = 100$, $k_BT = 1$, and the statistical segment length of the polymer $a = 1$ in all cases. Taking the typical diffusion coefficient for a polymer melt to be $D = 10^{-15}-10^{-13}$ cm^2/s and the statistical segment length a to be 1 nm, the time step of the simulation $a^2/(Mk_BT) = a^2/D$ corresponds to be about 0.1−10 s. Obviously, the microphases presented in this paper are subject to the 2D restriction in which one may not obtain those intrinsic 3D microstructures. However, we believe that the 2D calculation is able to catch the essential feature of the ordering mechanism since it is determined only by the segregation sequence of the species. The results presented here for each triblock copolymer were averaged for five times with different initial conditions. To describe the composition of the triblock copolymers, we use the $A_xB_yC_z$ nomenclature, where the subscripts x, y, and z are the average volume fraction of the A, B, and C species, respectively. The morphology is represented in the form of density plots with the intensity proportional to the local volume fraction of the species. Three different colors, blue, green, and red, are assigned to A, B, and C blocks, respectively.

A. Equilibrium Morphology of Linear ABC Triblock Copolymers. Before investigating the ordering mechanism of the linear ABC triblock copolymers, the DDFT is applied to predict their 2D equilibrium morphology and compared to experiments and other theories. The equilibrium morphology in each run is determined when the free energy of the system becomes constant after long enough time. Furthermore, for each set of parameters, several runs were taken with different initial random conditions to ensure that the exact equilibrium morphology has been obtained.

Figure 2 shows all 2D equilibrium microphases obtained by DDFT, which can be classified into two groups: classical and complex microphases. The former group includes the hexagonal lattice phase (HEX), core−shell hexagonal lattice phase (CSH), and "three-color" lamellar phase (LAM_3). The HEX phase (Figure 2a) is obtained with the majority species forming the matrix, while the two minority species being mixed together to form the hexagonal lattice. The same morphology was also found by Tang et al. with the same composition using SCFT.[8] Another characteristic morphology of the triblock copolymers, the CSH phase (Figure 2b), is in agreement with the experimental findings.[4,36] The LAM_3 phase (Figure 2c) is formed when the volume fraction of the three species are comparable. The LAM_3 phase was also predicted by the strong segregation theory[7] and the SCFT[8] and was indeed observed recently in a poly(styrene-*b*-isoprene-*b*-ethylene oxide) melt.[37] The latter group of microphases includes the two interpenetrating tetragonal lattice phase (TET_2), lamellar phase with beads inside (LAM + BD-I), tetragonal phase with beads at interface (TET + BD), and lamellar phase with beads at interface (LAM + BD-II). The TET_2 phase (Figure 2d) consists of two interpenetrating tetragonal lattices of A- and C-rich spheres embedded in a matrix of B. There are also experiments[3,38] and theoretical results[29] showing a similar phase. The LAM + BD-I phase (Figure 2e) is also found in the DDFT calculation, which agrees with the theoretical prediction of Zheng and Wang[7] and recent experiments by Krausch.[39] The TET + BD phase (Figure 2f) and LAM + BD-II phase (Figure 2g) can be compared with the experimental findings by Stadler et al.,[40] who studied a poly(styrene-*b*-butadiene-*b*-methyl methacrylate) (PS−PB−PMMA) triblock copolymer, in which PS and PMMA are weakly incompatible while they both show a pronounced incompatibility toward PB. It was found that the PB midblock (7 and 12 wt %) forms helical strands surrounding the PS cylinders (25 and 26 wt %) that are imbedded in the PMMA matrix, which is an intrinsic 3D structure. However, if the ultrathin section was along the main axis of the PS cylinders, a structure similar to the LAM + BD-II phase was observed, while if the section was perpendicular to the PS cylinders, the TET + BD phase was obtained.

B. Ordering Mechanism of Linear ABC Triblock Copolymers. In the ordering process of block copolymers quenched from a disordered state, it is the competition between the internal energy and entropic stretching energy that drives the system to an equilibrium state with the lowest free energy. To quantitatively measure the segregating sequence of the three species, we introduce order parameters S_{IJ} to describe the degree of phase separation between each pair of species:

$$S_{IJ} = \frac{C_n}{V}\int d\mathbf{r} \left|\left[\phi_I(\mathbf{r}) - \frac{f_I}{1 + (\phi_K(\mathbf{r}) - f_K)}\right] - \left[\phi_J(\mathbf{r}) - \frac{f_J}{1 + (\phi_K(\mathbf{r}) - f_K)}\right]\right| \quad (14)$$

where C_n is a normalization constant

$$\frac{1}{C_n} = \frac{4f_I f_J}{1 - f_K} + \frac{f_K|f_I - f_J|}{2 - f_K} \quad (15)$$

where $(I, J, K) \in \{(A, B, C),(C, A, B),(B, C, A)\}$, $\phi_I(\mathbf{r})$ is the density field of the corresponding species I, and f_I is the average volume fraction of the species I in volume V. $S_{IJ} = 0$ when the two species I and J are completely mixed, while $0 < S_{IJ} \leq 1$ when they are unmixed, and the equality holds when the two species phase separate completely. Therefore, S_{IJ} is a measure of the degree of phase separation between I and J and is determined by the product $\chi_{IJ}N$, where χ_{IJ} is the Flory−Huggins parameter and N is the chain length.

In the mean-field approximation, the parameters that determine the morphology of the triblock copolymers are the volume fractions f_I, the Flory−Huggins interaction parameters χ_{IJ} (in fact the combined parameters $\chi_{IJ}N$), and the topological structures of the block copolymers.[4,8] To facilitate examining the effect of these parameters on the phase ordering mechanism in the triblock copolymers, we group the system into two classes in terms of the χ parameters: one with symmetric interaction parameters ($\chi_{AB} = \chi_{BC} = \chi_{AC}$) and the other with asymmetric interaction parameters ($\chi_{AB} \neq \chi_{BC} \neq \chi_{AC}$).

B.1. Symmetric Interaction Parameters. We first consider the case of equal interaction energies between each species ($\chi_{AB} = \chi_{BC} = \chi_{AC} = 0.35$), in which the effect of the volume fraction on the ordering mechanism of ODT is highlighted. Two typical compositions of the linear triblock copolymer, $A_{0.33}B_{0.33}C_{0.34}$ and $A_{0.6}B_{0.2}C_{0.2}$, which respectively represent symmetric and asymmetric compositions, are chosen as examples to explore the ordering mechanism.

Figure 3a shows the time evolution of the morphology for the symmetric triblock copolymer $A_{0.33}B_{0.33}C_{0.34}$ quenched from a disordered state at time $t = 0$ to a state with $\chi_{AB} = \chi_{BC} = \chi_{AC} = 0.35$. It is observed that at early time, $t \leq 100$, the three species A (blue color), B (green color), and C (red color) simultaneously separate from each other, which corresponds to the one-step ordering mechanism M_I. In the intermediate stage, $t = 500$, both the domain size and the intensity difference of each block increase, with many structural defects trapped in the system, which is typical in this stage of microphase separation. At later stage of the ordering process, an ordered LAM_3 structure is formed with lamellae widths $D_A = D_C \simeq 2D_B$.

The time evolution of the order parameters S_{AB}, S_{BC}, and S_{AC}, for the system $A_{0.33}B_{0.33}C_{0.34}$ quenched at $\chi_{AB} = \chi_{BC} = \chi_{AC} = 0.35$, is shown in Figure 3b. In the early stage (with $t \leq 100$), fast increase of the three order parameters reflects a rapid domain formation process. Indeed, the study of the microphase separation of poly(styrene-*b*-butadiene) in a semidilute solution by time-resolved small-angle X-ray scattering demonstrated that the ordering occurs fast in a very early stage which only lasts with a time period of the order of 10^2 s.[41] Our DDFT calculation shows the rapid increase of the order parameters occurs at a time scale less than 10^2 time steps, corresponding to be $10-10^3$ s if typical values of statistical segment length and segment mobility coefficient are used. Furthermore, in this stage the slopes of the evolution curves of the three order parameters are almost equal, which means that the three species separate from each other simultaneously, corresponding to the one-step ordering mechanism, M_I.

In the later stages of the ordering process, the order parameters only increase gradually with the domains adjusting themselves to form more ordered structures. Recently, such distinct regimes of phase ordering kinetics of a triblock copolymer were identified by dynamic mechanical analysis experiments,[42] which experienced an initial rapid increase of the modulus when quenched from the disordered state, followed by a slower change of the modulus in the ordering process.

We also note S_{AB} and S_{BC} are almost equal, while S_{AC} is higher than both of them but slightly lower than 1, approaching the limit of complete unmixing of the species A and C. In the intermediate-segregation region, with the increase of χN, the local volume fraction of the majority species in each domain reaches larger values and the domain spacing increases as well. Therefore, the reason that S_{AB} and S_{BC} are equal at late stage is because $f_A = f_C$ and $\chi_{AB} = \chi_{BC}$, while the higher value of S_{AC} origins from the two end blocks (A and C) forming two distinct domains separated by the middle block B; i.e., there are no interfaces between the domains A and C. Note that at time $t = 2260$ the three order parameters all have sudden increase and form steps on the profiles of the order parameter evolution, corresponding to the rearrangement of the microstructures to form a perfect LAM_3 phase. These inflections are similar to the discontinuity of the order parameters observed in OOT. However, we attribute these inflections to the sudden disappearance of the unfavorable interfaces (corresponding to the number of contacts between dissimilar A and C monomers, see the morphology at $t = 2260$ before the inflection and $t = 2500$ after the inflection).

To further investigate the effect of composition on the ordering mechanism, we consider an asymmetric triblock copolymer $A_{0.6}B_{0.2}C_{0.2}$. Figure 4a shows the time evolution of the morphology for this asymmetric triblock quenched to $\chi_{AB} = \chi_{BC} = \chi_{AC} = 0.35$ from a disordered state at time $t = 0$. It is observed that, at an early time of $t = 50$, the A domains (which are in blue) separate from the B (green) and C (red) mixed phases, followed by the further unmixing of the B and C species later. Such ordering mechanism corresponds to the two-step ordering mechanism M_{IIA}. In the intermediate state, $t = 500$, a CSH phase starts to emerge and the C blocks form the core. At later stage of the ordering, an ordered CSH structure is formed with the majority species A as matrix, while one of the minority species, the C block, forming the inner cores, and the middle block B forming the shells in between the matrix and the cores.

Figure 4b shows the corresponding time evolution of the order parameters S_{AB}, S_{BC}, and S_{AC} for the system $A_{0.6}B_{0.2}C_{0.2}$. In the early stage with $t \leq 100$, similar to one observed in the symmetric case, the emerging of the domains leads to drastic increases of the order parameters. The time scale of this period is also about 10^2 simulation steps. In this stage, the slopes of the order parameter profiles for S_{AB} and S_{AC} are almost equal, but are both greater than that for S_{BC}, in agreement with the mechanism that the A domains separate from

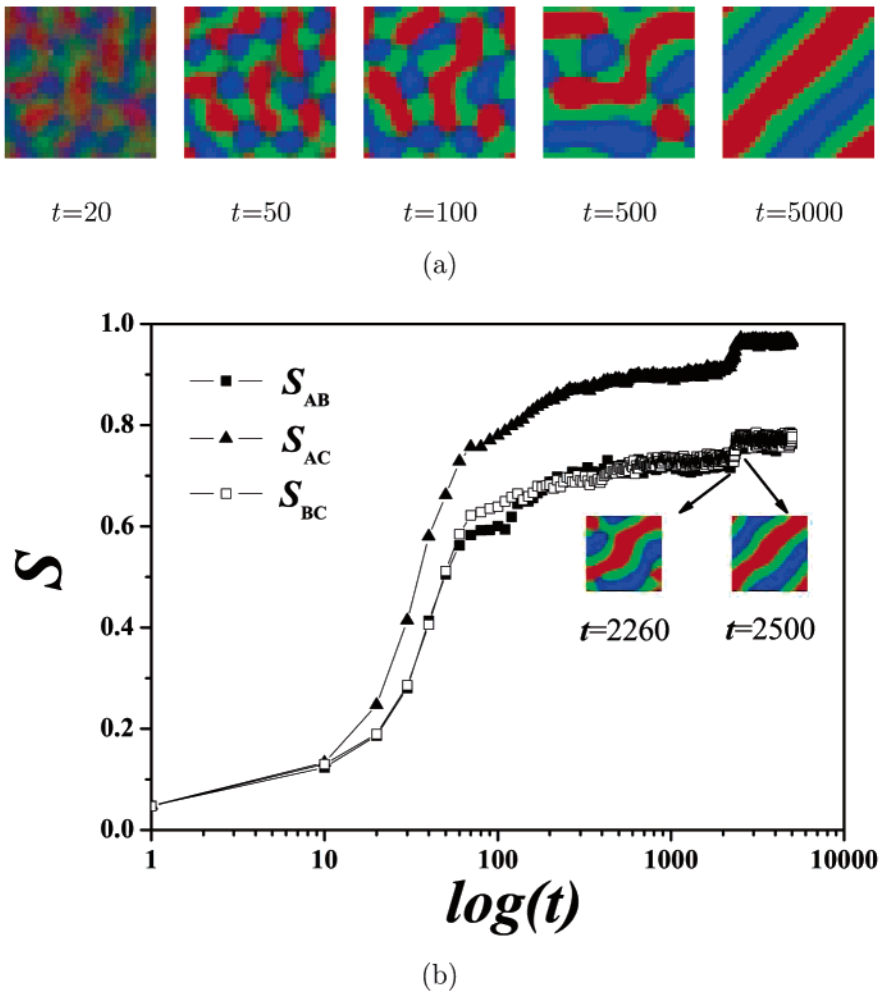

Figure 3. (a) Time evolution of the 2D morphology for the triblock copolymer $A_{0.33}B_{0.33}C_{0.34}$ at time t = 20, 50, 100, 500, and 5000. Three different colors, blue, green, and red, are assigned to A, B, and C blocks, respectively. The Flory−Huggins interaction parameters are set to be $\chi_{AB} = \chi_{BC} = \chi_{AC} = 0.35$ and the chain length $N = 100$. (b) Time evolution of the order parameters. In the inset, the morphology for t = 2260 and 2500 is shown.

the mixed B and C species first, followed by the B and C unmixing, i.e., the ordering mechanism M_{IIA}.

Following the fast process is also a rather steady evolution of the order parameters. Differing from the $A_{0.33}B_{0.33}C_{0.34}$ system, however, there is no inflections on the profiles of any of the order parameters. The reason is that the unfavorable interfaces have already disappeared in the early stage of the microphase separation, judging from the morphology evolution for this asymmetric case (compare the morphology for t = 300 and 4000 in Figure 4b). In the later stage, S_{AC} is higher than both S_{AB} and S_{BC}, which is because the A and C domains are separated by the B shell, favoring the unmixing of the A and C species. While S_{BC} is much lower than S_{AB}, this is because $f_C < f_A$; i.e., the effective chain length of the B and C blocks is shorter than that of the A and B. Therefore, although with the same interaction energies, the ordering mechanism may vary with the composition of the triblock copolymers.

By systematically varying the composition, mechanism diagrams can be constructed for the ABC triblock polymers. A triangle diagram of the system with equal interaction parameters $\chi_{AB} = \chi_{BC} = \chi_{AC} = 0.35$ is shown in Figure 5. In the center region of the phase diagram, where the volume fractions of the three species are comparable, microphase separation of the triblock copolymer from the disordered state adopts the ordering mechanism M_I. At the corner of A (where the A species dominates), the ordering mechanism is M_{IIA}. Correspondingly, the ordering mechanism is M_{IIC} at the C corner of the diagram. However, at the B corner, the triblock copolymer does not phase separate with the present χ values. (Increasing the χ values eventually can lead to an M_I mechanism at this corner.) On the AC edge of the triangle diagram, the ordering mechanism is also M_I, which means that the minority component (the middle block B) separates simultaneously with the two majority components. This can be attributed to the connection of the middle B block to both of the two end blocks, which enhances the trend of the B species to unmix with the other two. Recently, it was reported that the microphase separation between polyisoprene (PI) and poly(deuterated styrene) (DPS) was enhanced due to one end of DPS tethered with poly(vinyl methyl ether) (PVME) in the triblock copolymer poly(isoprene-*b*-deuterated styrene-*b*-vinyl methyl ether).[43] On the rest two edges (AB, BC) of the triangle diagram, only two-phase morphologies exist at the equilibrium state with the exceptions near the corners of A and C, where the ordering mechanisms are M_{IIA} and M_{IIC}, respectively.

B.2. Asymmetric Interaction Parameters. In this section, we study the ordering mechanism of the triblock copolymers with unequal interaction energies between each species. We choose a typical triblock copolymer

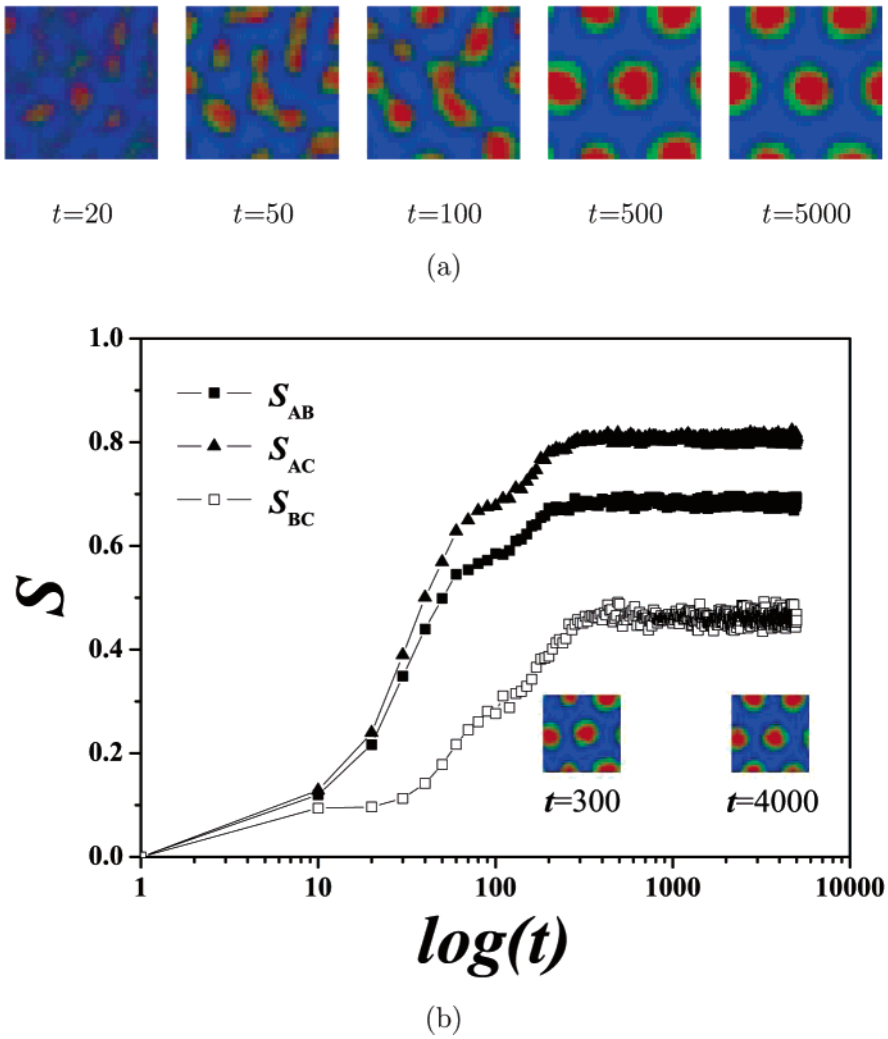

Figure 4. (a) Time evolution of the 2D morphology for the triblock copolymer $A_{0.6}B_{0.2}C_{0.2}$ at time t = 20, 50, 100, 500, and 5000. Three different colors, blue, green, and red, are assigned to A, B, and C blocks, respectively. The Flory−Huggins interaction parameters are set to be $\chi_{AB} = \chi_{BC} = \chi_{AC} = 0.35$ and the chain length $N = 100$. (b) Time evolution of the order parameters. In the inset, the morphology for t = 300 and 4000 is shown.

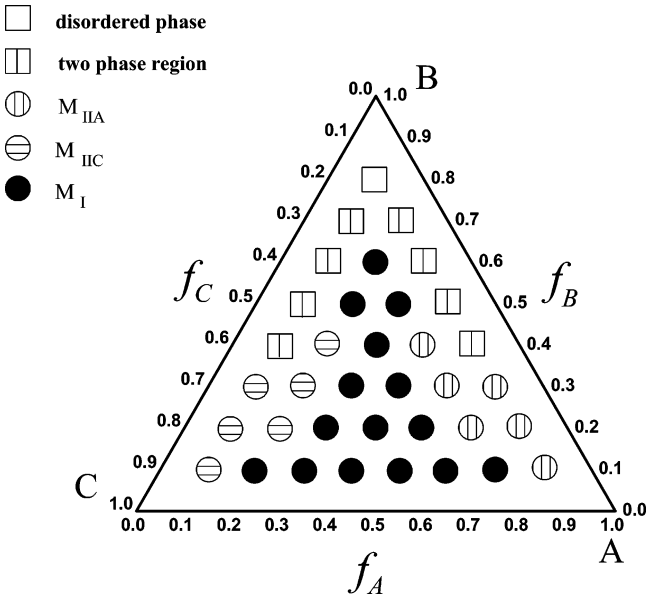

Figure 5. Triangle ordering mechanism diagram for linear ABC triblock copolymers with $\chi_{AB} = \chi_{BC} = \chi_{AC} = 0.35$.

with $\chi_{AC} \ll \chi_{AB} \approx \chi_{BC}$, which means the middle block B is more incompatible to the two end blocks (A and C). Such systems, including poly(styrene-*b*-butadiene-*b*-methyl methacrylate) (SBM) and poly(styrene-*b*-ethylene-*co*-butylene-*b*-methyl methacrylate) (SEBM), have been extensively studied in previous experiments to explore the possible complex morphologies.[19,40] More specifically, we set $\chi_{AB} = 0.50$, $\chi_{BC} = 0.48$, and $\chi_{AC} = 0.20$. Figure 6 shows the time evolution of the order parameters, S_{AB}, S_{BC}, and S_{AC}, for a compositional symmetric triblock $A_{0.33}B_{0.33}C_{0.34}$. In the early stage, $t \leq 200$, the slopes of the evolution for the order parameters S_{AB} and S_{BC} are almost equal but are greater than that for S_{AC}. This corresponds to the M_{IIB} mechanism, in which the B species segregate from the mixed A and C first, followed by the separation of the two mixed phases. At the later stage of the microphase separation, S_{AC} is lower compared to its value in the system with equal interaction parameters, resulting from the weaker interaction energy between A and C blocks.

The mechanism diagram of the ordering process for such triblock polymer is shown in Figure 7. In the center region of the diagram, due to the stronger incompatibility of the middle block B toward the two end blocks A and C, ordering mechanism changes to M_{IIB}, as compared to the system with symmetric interaction parameters. At the A corner of the diagram, the ordering mechanism is still M_{IIA}. Correspondingly, at the corner

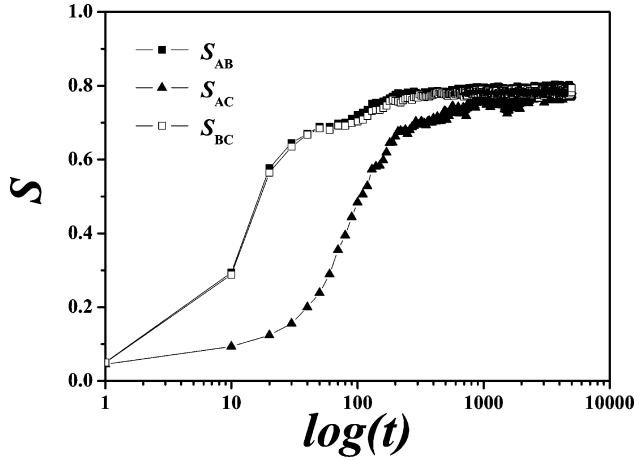

Figure 6. Time evolution of the order parameters of the triblock copolymer $A_{0.33}B_{0.33}C_{0.34}$ with $\chi_{AB} = 0.50$, $\chi_{BC} = 0.48$, and $\chi_{AC} = 0.20$.

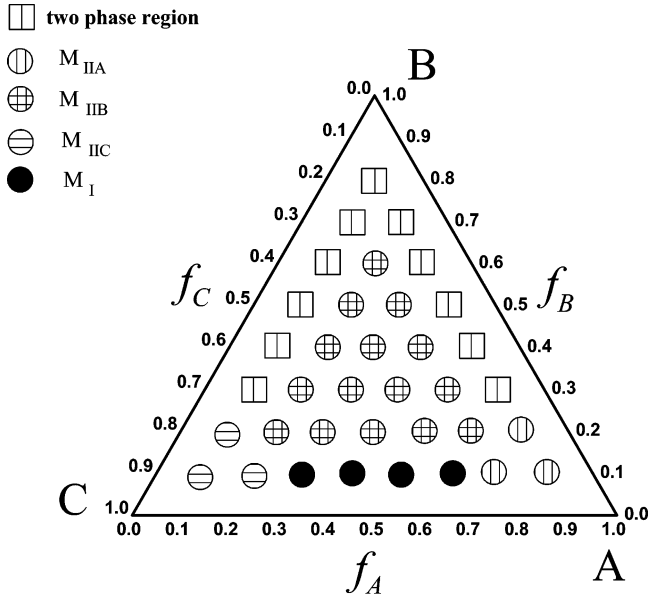

Figure 7. Triangle ordering mechanism diagram for linear ABC triblock copolymers with $\chi_{AB} = 0.50$, $\chi_{BC} = 0.48$, and $\chi_{AC} = 0.20$.

of C, the order mechanism of the triblock is M_{IIC}. At the corner of B, however, the triblock forms a two-phase equilibrium state. Near the AC edge of the triangle diagram, the ordering mechanism M_I appears only at the center, while in the other part of this edge, the ordering mechanism is either M_{IIA} or M_{IIC}. At the rest two edges (AB, BC) of the triangle diagram, the equilibrium morphology is two-phase except near the corners of A and C.

A distinctively new feature absent in diblock copolymers arises in triblock copolymers: the microphase separation may depend on the sequence of the blocks, i.e., whether it is sequenced A−B−C, B−C−A, or C−A−B. Taking the previously investigated triblock with $\chi_{AC} \ll \chi_{AB} \approx \chi_{BC}$ as an example, if the end block A is switched with the middle block B and rename it again as ABC, the interaction parameters between each species change to $\chi_{AC} \approx \chi_{AB} \gg \chi_{BC}$; i.e., the end block A is more unfavorable to the middle block B and another end block C. The mechanism diagram of the ordering process for the triblock with such switched sequence is shown in Figure 8. Compared to Figure 7, the ordering

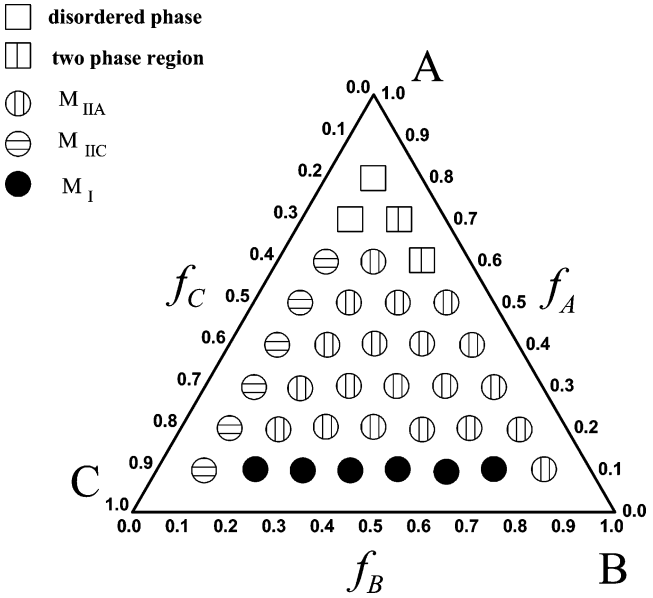

Figure 8. Triangle ordering mechanism diagram for linear ABC triblock copolymers with $\chi_{AB} = 0.50$, $\chi_{BC} = 0.20$, and $\chi_{AC} = 0.48$.

mechanism in most region changes to M_{IIA} because the A block are strongly incompatible to the other two. Near the AC edge, the region of M_I expands. Switching the sequence also leads to a reduction of the two-phase region.

IV. Conclusions

We have studied the ordering mechanism for the disorder-to-order transition in linear triblock copolymers by means of dynamic density functional theory (DDFT). We verified the implementation of the DDFT by searching 2D equilibrium morphologies of the linear triblock copolymer and comparing the output with that of the self-consistent-field theory (SCFT) and previous experiments. For ABC linear triblock copolymers quenched from a disordered state, in general the ordering dynamics involves a fast initial phase segregation followed by an extremely slow defect annihilation process. This result agrees with the experimental observation of Cochran et al.[42] The time evolution of the phase structures and corresponding order parameters were obtained in the DDFT simulation.

A careful examination of the morphologies and order parameters reveals that the mechanisms of the complex ordering in ABC triblock copolymers can be divided into two types: the one-step mechanism M_I, in which all the three species segregate simultaneously after the system is quenched from a disordered state, and the two-step mechanism M_{II}, in which segregation of one species from the other two occurs first, followed by separation of the two mixed species. When the volume fraction of one species dominates the other two, the phase ordering always proceeds through a two-step mechanism with the majority one segregating at first, provided a three-phase morphology formed at the end. When the volume fractions of the three species are comparable, the ordering mechanism depends on the interaction energies among them: for the symmetric interaction case, the microphase separation occurs through an one-step mechanism, while for the asymmetric interaction case, it occurs through a two-step mechanism with the most incompatible species segregating at first.

The present DDFT study shows that a two-step microphase separation can be achieved by simply quenching a triblock copolymer from the disordered state into an ordered state (only one temperature jump is needed), instead of changing the interaction energies among different species through continuously varying temperature (many adjustments to temperature) or adding a selective solvent. To facilitate the numerical calculation, this idea is demonstrated only in two-dimensional space; we nevertheless believe it is also applicable in 3D. The reason is that, for the disorder-to-order transition, the ordering mechanism is determined in a rather early stage, in which the dominant process is the segregation of the different species, not the spatial reorganization of the domains. We however are aware that for an order-to-order transition the spatial dimension is crucial because intrinsic 3D microphases might be involved in the phase ordering process, which only can be investigated by 3D calculations.

Note Added in Proof. After submission of our manuscript, we learned about an experiment on molten ABC triblock copolymers by Corte et al.,[44] in which a microphase separation mechanism that was similar to the two-step mechanism was discussed.

Acknowledgment. We gratefully acknowledge financial support from the Special Funds for Major State Basic Research Projects and the National Natural Science Foundation of China (Grants 20374016, 20234010, 20221402, and 20490220). F.Q. acknowledges the Ministry of Education of China (FANEDD 200225) and the STCSM (Grant 02QE14010).

References and Notes

(1) Hamley, I. W. *Nanotechnology* **2003**, *14*, R39.
(2) Bates, F. S.; Schulz, M. F.; Khandpur, A. K.; Förster, S.; Rosedale, J. H.; Almdal, K.; Mortensen, K. *Faraday Discuss.* **1994**, *98*, 7.
(3) Mogi, Y.; Kotsuji, H.; Kaneko, Y.; Mori, K.; Matsushita, Y.; Noda, I. *Macromolecules* **1992**, *25*, 5408.
(4) Gido, S. P.; Schwark, D. W.; Thomas, E. L.; Goncalves, M. D. *Macromolecules* **1993**, *26*, 2636.
(5) Leibler, L. *Macromolecules* **1980**, *13*, 1602.
(6) Matsen, M. W.; Schick, M. *Phys. Rev. Lett.* **1994**, *72*, 2660.
(7) Zheng, W.; Wang, Z. G. *Macromolecules* **1995**, *28*, 7215.
(8) Tang, P.; Qiu, F.; Zhang, H. D.; Yang, Y. L. *Phys. Rev. E* **2004**, *69*, 031803.
(9) Bates, F. S.; Fredrickson, G. H. *Phys. Today* **1999**, *52*, 32.
(10) Tyler, C. A.; Morse, D. C. *Phys. Rev. Lett.* **2005**, *94*, 208302.
(11) Almdal, K.; Koppi, K. A.; Bates, F. S.; Mortensen, K. *Macromolecules* **1992**, *25*, 1743.
(12) Förster, S.; Khandpur, A. K.; Zhao, J.; Bates, F. S.; Hamley, I. W.; Ryan, A. J.; Bras, W. *Macromolecules* **1994**, *27*, 6922.
(13) Khandpur, A. K.; Förster, S.; Bates, F. S.; Hamley, I. W.; Ryan, A. J.; Bras, W.; Almdal, K.; Mortensen, K. *Macromolecules* **1995**, *28*, 8796.
(14) Kimishima, K.; Koga, T.; Hashimoto, T. *Macromolecules* **2000**, *33*, 968.
(15) Bahiana, M.; Oono, Y. *Phys. Rev. A* **1990**, *41*, 6763.
(16) Qi, S.; Wang, Z. G. *Phys. Rev. Lett.* **1996**, *76*, 1679.
(17) Ren, S. R.; Hamley, I. W. *Macromolecules* **2001**, *34*, 116.
(18) Auschra, C.; Stadler, R. *Macromolecules* **1993**, *26*, 2171.
(19) Breiner, U.; Krappe, U.; Thomas, E. L.; Stadler, R. *Macromolucules* **1998**, *31*, 135.
(20) Hardy, C. M.; Bates, F. S.; Kim, M. H.; Wignall, G. D. *Macromolecules* **2002**, *35*, 3189.
(21) Yamauchi, K.; Hasegawa, H.; Hashimoto, T.; Köhler, N.; Knoll, K. *Polymer* **2002**, *43*, 3563.
(22) Yamauchi, K.; Hasegawa, H.; Hashimoto, T.; Nagao, M. *J. Appl. Crystallogr.* **2003**, *36*, 708.
(23) Maniadis, P.; Thompson, R. B.; Rasmussen, K. Ø.; Lookman, T. *Phys. Rev. E* **2004**, *69*, 031801.
(24) Fraaije, J. G. E. M. *J. Chem. Phys.* **1993**, *99*, 9202.
(25) Fraaije, J. G. E. M.; van Vlimmeren, B. A. C.; Maurits, N. M. *J. Chem. Phys.* **1997**, *106*, 4260.
(26) Reister, E.; Müller, M.; Binder, K. *Phys. Rev. E* **2001**, *64*, 041804.
(27) Yeung, C.; Shi, A. C. *Macromolecules* **1999**, *32*, 3637.
(28) Morita, H.; Kawakatsu, T.; Doi, M.; Yamaguchi, D.; Takenaka, M.; Hashimoto, T. *Macromolecules* **2002**, *35*, 7473.
(29) Nakazawa, H.; Ohta, T. *Macromolecules* **1993**, *26*, 5503.
(30) Hohenberg, P. C.; Halperin, B. I. *Rev. Mod. Phys.* **1977**, *49*, 435.
(31) Morita, H.; Kawakatsu, T.; Doi, M. *Macromolecules* **2001**, *34*, 8777.
(32) Helfand, E. *J. Chem. Phys.* **1975**, *62*, 999.
(33) Edwards, S. F. *Proc. Phys. Soc.* **1965**, *85*, 613.
(34) Maurits, N. M.; van Vlimmeren, B. A. C.; Fraaije, J. G. E. M. *Phys. Rev. E* **1997**, *56*, 816.
(35) Ferreira, P. G.; Ajdari, A.; Leibler, L. *Macromolecules* **1998**, *31*, 3994.
(36) Breiner, U.; Krappe, U.; Abetz, V.; Stadler, R. *Macromol. Chem. Phys.* **1997**, *198*, 1051.
(37) Bailey, T. S.; Hardy, C. M.; Epps, T. H.; Bates, F. S. *Macromolecules* **2002**, *35*, 7007.
(38) Mogi, Y.; Mori, K.; Kotsuji, H.; Matsushita, Y.; Noda, I. *Macromolecules* **1994**, *27*, 6755.
(39) Ludwigs, S.; Böker, A.; Abetz, V.; Müller, A. H. E.; Krausch, G. *Polymer* **2003**, *44*, 6815.
(40) Stadler, R.; Auschra, C.; Beckmann, J.; Krappe, U.; Voigtmartin, I.; Leibler, L. *Macromolecules* **1995**, *28*, 3080.
(41) Gupta, J. A.; Singh, M. A.; Salomons, G. J.; Foran, W. A.; Capel, M. S. *Macromolecules* **1998**, *31*, 3109.
(42) Cochran, E. W.; Morse, D. C.; Bates, F. S. *Macromolecules* **2003**, *36*, 782.
(43) Hashimoto, T.; Yamauchi, K.; Yamaguchi, D.; Hasegawa, H. *Macromol. Symp.* **2003**, *201*, 65.
(44) Corte, L.; Yamauchi, K.; Court, F.; Cloitre, M.; Hashimoto, T.; Leibler, L. *Macromolecules* **2003**, *36*, 7695.

MA051355B